Received: 30 October 2017 | Revised: 2 January 2018 | Accepted: 5 January 2018

DOI: 10.1002/aoc.4297

FULL PAPER

WILEY Applied Organometallic Chemistry

Dinuclear Cu(II) complexes based on *p*-xylylene-bridged bis(1,4,7-triazacyclononane) ligands: Synthesis, characterization, DNA cleavage abilities and evaluation of superoxide dismutase- and catalase-like activities

Qi Tang[†] | Ji-Qing Wu[†] | Hong-Yan Li | Yan-Fang Feng | Zhong Zhang | Yu-Ning Liang

Key Laboratory for Chemistry and Molecular Engineering of Medicinal Resources (Ministry of Education of China), School of Chemistry and Pharmacy of Guangxi Normal University, Guilin, People's Republic of China

Correspondence
Zhong Zhang and Yu-Ning Liang, School of Chemistry and Pharmacy of Guangxi Normal University, Key Laboratory for Chemistry and Molecular Engineering of Medicinal Resources (Ministry of Education of China), Guilin, People's Republic of China.
Email: zhangzhong@mailbox.gxnu.edu.cn; liangyuning008@163.com

Funding information
National Natural Science Foundation of China, Grant/Award Number: 21361004; Guangxi Natural Science Foundation of China, Grant/Award Numbers: 2017GXNSFAA198125 and 2014GXNSFAA118044; Natural Science Foundation of Key Laboratory for Chemistry and Molecular Engineering of Medicinal Resources (Guangxi Normal University), Ministry of Education of China, Grant/Award Number: CMEMR2012-A08, CMEMR2013-C08

Three new dinuclear Cu(II) complexes with the formulas $[Cu_2(pxdmbtacn)Cl_4]$ (**1**), $[Cu_2(pxdmbtacn)Cl_{0.7}(NO_3)_{1.3}(OH)_2(H_2O)_{1.3}]\cdot 6H_2O$ (**2**) and $[Cu_2(pxdiprbtacn)Cl_4]$ (**3**) together with one previously reported complex, $[Cu_2(pxbtacn)Cl_4]$ (**4**), were obtained from Cu(II) salts with three *p*-xylylene-bridged bis-tacn ligands bearing pendant alkyl substituents or without pendant group. Complex **2** was structurally characterized as a centrosymmetric dinuclear molecule with each metal center being coordinated to some labile ligands in addition to one tacn ring. Based on the results of mass spectrometry and UV–visible spectroscopy, complexes **1** and **3** are capable of existing in aqueous solution as dinuclear species but **4** can partially form a dimer of the original dinuclear motif. Complexes **1**, **3** and **4** can all effectively cleave supercoiled DNA oxidatively in the presence of hydrogen peroxide. The superoxide dismutase (SOD) activities of **1** and **3** measured under physiological conditions are comparable to that of the native CuZnSOD enzyme but the enzymatic activity of **4** is about three- to fourfold lower. Furthermore, complexes **1**, **3** and **4** demonstrate moderate scavenging effect on hydrogen peroxide and their catalase activities are in the decreasing order of **3** > **1** > **4**.

KEYWORDS
catalase mimic, copper(II) complex, nuclease activity, SOD mimic, triazacyclononane

1 | INTRODUCTION

Reactive oxygen species (ROS) such as superoxide radical ($O_2^{\bullet -}$) and hydrogen peroxide (H_2O_2), generated from the direct reduction of molecular O_2 during the respiratory event, are known to induce cellular damage at elevated concentrations and have been proved to play a vital role in aging as well as in a number of diseases associated with oxidative stress.[1–7] For these reasons, the elimination of excess amounts of these reactive species from organisms is of great importance to prevent the occurrence of various diseases including neurological disorders and cancer. Superoxide dismutases (SODs) and catalases are the chief members of the natural antioxidant defense system helping to limit the accumulation of the deleterious $O_2^{\bullet -}$ and H_2O_2. The former plays an essential role

[†]These authors contributed equally to this work.

in conversion of superoxide anion to hydrogen peroxide and oxygen under physiological conditions, and the latter is able to catalyze the decomposition of hydrogen peroxide into water and oxygen.[8–12]

For a variety of diseases related to a deficiency of these native antioxidant enzymes, the use of exogenous SODs and catalases has been firstly considered as a feasible therapeutic approach.[13–15] However, the immunogenic response, short lifetime and lower tissue permeability of these high-molecular-mass materials make them difficult to be used *in vivo* for therapeutic application.[16,17] This spurred researchers to look for biomimetic small-molecule compounds which can degrade $O_2^{\bullet-}$ or H_2O_2 effectively as promising substitutes of native enzymes.[18–22] Recently, numerous and diverse redox-active transition metal complexes based on N-donor ligands have been reported to exhibit marked catalytic effect on the disproportionation of reactive $O_2^{\bullet-}$ or H_2O_2 *in vitro*[23–27] and some pentaazamacrocyclic Mn(II) compounds as antioxidant SOD mimics have found biomedical applications in preclinical or clinical trials.[28–31] As a facially coordinated tridentate macrocycle, 1,4,7-triazacyclononane (tacn) and its derivatives are apt to construct thermodynamically stable and kinetically inert metal complexes, and some of these compounds have manifested an ability to cleave DNA or protein.[32–37] In the past two decades, several Cu(II) or Mn(II) complexes containing N-functionalized mono-tacn ligands with unsaturated or labile binding sites have been reported to show a considerable antioxidant effect on the scavenging of superoxide radical in the physiological environment.[38–46] It is anticipated that more efficacious model compounds of SODs will be obtained from bis-tacn (or multi-tacn) ligands which possess two or more active centers for the binding of substrate. Nevertheless, a mononuclear Cu(II) complex of a bis-tacn ligand bearing a flexible ethylene spacer has been prepared by Li *et al*., and it exhibited only a low SOD activity due to the saturated coordination environment around the central metal furnished by macrocyclic nitrogen atoms.[47] This result hints that rigid or semi-rigid spacers should be introduced into the bis-tacn (or multi-tacn) ligands to facilitate the formation of dinuclear (or polynuclear) metal compounds. Since SOD mimics usually produce toxic hydrogen peroxide during the catalytic cycles by a ping-pong mechanism, the mimicking compounds exhibiting both SOD- and catalase-like activities are intensively pursued which demonstrate special advantage over those merely having SOD activity.[48–50] Therefore, there is a growing requirement to develop small molecular mimics showing dual SOD/catalase activity to be used as antioxidant drugs.

In the work reported herein, four dinuclear Cu(II) complexes, $[Cu_2(pxdmbtacn)Cl_4]$ (**1**), $[Cu_2(pxdmbtacn)Cl_{0.7}(NO_3)_{1.3}(OH)_2(H_2O)_{1.3}]\cdot 6H_2O$ (**2**), $[Cu_2(pxdiprbtacn)Cl_4]$ (**3**) and $[Cu_2(pxbtacn)Cl_4]$ (**4**), were prepared from *p*-xylylene-bridged ditopic bis-tacn derivatives bearing steric alkyl substituents (pxdmbtacn = 1,4-bis(4,7-dimethyl-1,4,7-triazacyclonon-1-ylmethyl)benzene, pxdiprbtacn = 1,4-bis(4,7-diisopropyl-1,4,7-triazacyclonon-1-ylmethyl) benzene) or no pendant group (pxbtacn = bis(1,4,7-triazacyclonon-1-ylmethyl)benzene) (Figure 1). The magnetic, redox and spectroscopic properties of complexes **1**, **3** and **4** were investigated in detail. All three complexes can oxidatively degrade supercoiled pBR322 DNA with the help of H_2O_2. Furthermore, these complexes also exhibit catalytic activity towards the dismutation of $O_2^{\bullet-}$ and H_2O_2 functioning as dual SOD/catalase mimics. From the results obtained from these investigations, the different enzymatic activities of these complexes were related to the structural features of the bis-tacn ligands and the solution behavior of their complexes.

2 | EXPERIMENTAL

2.1 | Materials and Methods

All reagents were obtained from commercial sources and used without further purification. 1,4,7-Triazacyclononane was purchased from Wuxi Tongchuang Biotechnology Co. Ltd (China). Tris(hydroxymethyl)aminomethane, 4-(2-hydroxyethyl) piperazine-1-ethanesulfonic acid (HEPES), plasmid pBR322 DNA, loading buffer (10×), agarose, ethidium bromide (EB), xanthine, xanthine oxidase, nitroblue tetrazolium (NBT) and superoxide dismutase (CuZnSOD) from bovine erythrocytes were purchased from Sigma. All buffer solutions were prepared using triple-distilled water. All stock solutions were stored at 4 °C and used within 2 days. The H_2O_2 stock solution was prepared by diluting a commercial 30% aqueous solution and its concentration was determined by iodometric titration.[51]

Elemental analyses for C, H and N were conducted with an Elementar Vario Micro Cube elemental analyzer. Fourier transform infrared (FT-IR) spectra were recorded with a PerkinElmer Spectrum One spectrometer as KBr pellets in the 400–4000 cm^{-1} spectral region. Electrospray ionization mass spectrometry (ESI-MS) was performed

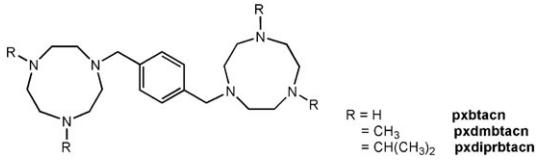

FIGURE 1 Structures of three *p*-xylylene-bridged bis-tacn ligands (R = H, CH_3, $CH(CH_3)_2$)

with a Bruker Esquire 3000 mass spectrometer. UV–visible spectra were acquired with a Varian CARY-100 spectrophotometer. Powder X-ray diffraction (PXRD) patterns for the as-synthesized samples were recorded using a Rigaku D/max-2500 V diffractometer with Cu Kα radiation ($\lambda = 1.54056$ Å) at 293 K in the 2θ range from 3° to 65°. Magnetic measurements were performed with a Quantum Design MPMS-XL7 magnetometer in the temperature range 2–300 K under a magnetic field of 2000 Oe. Diamagnetic corrections for sample and sample holder were applied using Pascal's constants. Electron spin resonance (ESR) spectra of powdered samples were recorded at room temperature with a Bruker EMX10/12 spectrometer operating at the X-band frequency (9.8 GHz) and magnetic field modulation of 100 kHz.

2.2 | Electrochemical Experiments

Cyclic voltammetry experiments were performed using a CHI 660D system under a nitrogen atmosphere in a three-electrode cell with a glassy carbon working electrode, a platinum wire auxiliary electrode and a saturated Ag/AgCl reference electrode. The complexes were dissolved in triple-distilled water and their concentrations were adjusted to 1.0×10^{-3} M. Tetra-*n*-butylammonium bromide (0.1 M) was used as the supporting electrolyte and the pH of the solution was close to 6.0. The half-wave potential ($E_{1/2}$) was calculated as the midpoint of the anodic (E_{pa}) and cathodic (E_{pc}) peak potentials: $E_{1/2} = (E_{pa} + E_{pc})/2$.

2.3 | DNA Cleavage Experiments

The DNA cleavage activities of the complexes were evaluated via agarose gel electrophoresis, which was conducted using the following procedure. Plasmid pBR322 DNA in HEPES buffer (pH = 6.8) was mixed with varying concentrations of complexes in the absence and presence of H_2O_2. The resulting mixture was incubated at 37 °C for 2 h in the dark, after which 2 μl of buffer was added to quench the reaction. Then the DNA samples were loaded on 2% agarose gel and electrophoresed at 70 V for 2 h in TAE buffer. The gel was stained with 0.1% EB, visualized by UV light and photographed. Control experiments were carried out using Cu(II) salts or the free ligands at a concentration of 12–24 μM in the absence and presence of H_2O_2, respectively.

The cleavage mechanism of pBR322 DNA induced by the complexes was investigated in the presence of various radical scavengers, namely C_2H_5OH, dimethylsulfoxide (DMSO), KI, NaN_3, L-histidine and SOD. All samples were treated by the same method described for DNA cleavage. The experiment was repeated three times to ensure consistency of the results.

2.4 | SOD-Like Activity Assays

The SOD-like activity was assessed by an indirect method originally developed by Beauchamps and Fridovich with some modifications.[52] Superoxide anions were generated by the xanthine–xanthine oxidase system and measured using the NBT method. The solutions containing xanthine (1.0×10^{-3} M), NBT (2.5×10^{-3} M) and various concentrations of the complexes were prepared with phosphate buffer (pH = 7.4, 0.01 M) at 25 °C. Sufficient xanthine oxidase was added to the solutions to produce a change in absorbance of 0.025 min^{-1} at 550 nm. The NBT reduction rate was measured in the presence and absence of various concentrations of the investigated complexes. Each complex was run in three parallel tests. The IC_{50} value (the concentration of the complex to cause 50% inhibition of NBT reduction) of each complex was acquired from the concentration-dependent inhibition curves and the relative activity represents the ratio of the measured activity of the native CuZnSOD to that of each complex under the same experimental conditions.

2.5 | Catalase-Like Activity Assays

The catalase-like activity was determined using the volumetric method. The dismutation reaction of H_2O_2 catalyzed by each complex was carried out at room temperature in a three-necked flask (250 ml) equipped with a magnetic stirrer and closed with a rubber septum. The flask was connected to an inverted graduated burette filled with water. Under stirring, the required volume of H_2O_2 stock solution was injected into an aqueous solution of the complex through the septum with a microsyringe. Volume of oxygen evolved was measured at certain time intervals and the experimental data were plotted as a curve describing the volume of oxygen evolved as a function of time. The initial rate of dioxygen evolution was expressed as mol(O_2) s^{-1} and obtained from the slope of the curve. The turnover number k_{cat}, the Michaelis constant K_M and k_{cat}/K_M were determined from the double-reciprocal Lineweaver–Burk plot obtained at a constant catalyst concentration. The experiment was repeated three times to ensure consistency of the results.

2.6 | X-ray Data Collection and Structure Determination

Diffraction data were collected at 296 K with graphite-monochromated Mo Kα radiation ($\lambda = 0.71073$ Å) using a Bruker Smart Apex II CCD diffractometer. The SAINT

program was used for integration of the diffraction profiles[53] and an empirical absorption correction was applied with the SADABS program.[54] The structure was solved by direct methods using the SHELXS program of the SHELXTL package and refined by full-matrix least squares on F^2 with the SHELXL program.[55] All non-hydrogen atoms were located in successive difference Fourier syntheses and refined with anisotropic thermal parameters on F^2. All of the hydrogen atoms attached to carbon atoms were placed in calculated positions and treated as riding atoms during the refinement. The hydrogen atoms attached to oxygen atoms were located from difference Fourier maps with O—H bond distances restrained to 0.85 Å and refined isotropically with $U_{iso}(H) = 1.5U_{eq}(O)$. CCDC 1582386 contains the supplementary crystallographic data for complex **2**. Crystallographic data and structural refinement details are summarized in Table 1. Selected bond lengths and angles are collected in Table 2. Hydrogen bond data are presented in Table S1.

2.7 | Synthesis of Ligands

2.7.1 | Bis(1,4,7-triazacyclonon-1-ylmethyl)benzene (pxbtacn)

The ligand pxbtacn was obtained according to the established method.[56]

2.7.2 | 1,4-Bis(4,7-dimethyl-1,4,7-triazacyclonon-1-ylmethyl)benzene (pxdmbtacn)

The oily precursor pxbtacn (2.0 mmol, 1.16 g) was dissolved in a mixture of formic acid (10 ml) and formaldehyde (10 ml) with stirring. The resulting solution was refluxed for 20 h and then cooled to room temperature. Subsequently, 20 ml of water was poured into the solution and its pH value was adjusted to about 12 by adding solid NaOH. After filtration, the filtrate was extracted with chloroform (5 × 50 ml) and the combined extracts were dried over anhydrous Na_2SO_4. The solvent was evaporated under reduced pressure to give a yellow oil. Yield: 4.60 g, 86%. FT-IR (KBr, cm^{-1}): 3422(s), 2943(m), 2852(m), 2813(m), 2703(m), 1663(s), 1464(s), 1382(s), 1294(m), 1184(m), 1117(m), 1079(m), 1062(m), 1032(m), 998(m), 898(w), 856(w), 829(w), 741(w), 596(w), 556(w), 499(w). ESI-MS: $m/z = 417.3$ $[M + H]^+$.

2.7.3 | 1,4-Bis(4,7-diisopropyl-1,4,7-triazacyclonon-1-ylmethyl)benzene (pxdiprbtacn)

To a solution of pxbtacn (3.2 mmol, 1.16 g) in dry acetonitrile (50 ml) was added solid K_2CO_3 (14.5 mmol, 2.00 g) and isopropyl bromide (25.6 mmol, 3.18 g) sequentially. The mixture was then refluxed for 20 h under a nitrogen atmosphere. After cooling the mixture to ambient temperature, the generated KBr and excess K_2CO_3 were removed by filtration. The filtrate was washed with chloroform (2 × 50 ml), and the combined filtrates were dried over anhydrous Na_2SO_4. Evaporating the solvent under reduced pressure yielded a pale yellow oil. Yield: 1.26 g, 74%. FT-IR (KBr, cm^{-1}): 3435(m), 2962(s), 2927(s), 2871(m), 2816(m), 1663(s), 1462(m), 1384(m), 1359(m), 1300(m), 1170(m), 1116(m), 1086(m), 1057(m), 1019(m), 838(w), 760(w), 705(w), 577(w), 492(w). ESI-MS: $m/z = 529.6$ $[M + H]^+$.

TABLE 1 Crystal data and structure refinement of complex **2**

Complex	2
Empirical formula	$C_{24}H_{60.59}Cl_{0.70}Cu_2N_{7.30}O_{13.18}$
Formula weight	814.36
Temperature (K)	296
Wavelength (Å)	0.71073
Crystal system	Monoclinic
Space group	$P2_1/n$
a (Å)	8.987(3)
b (Å)	13.289(4)
c (Å)	16.446(6)
α (°)	90
β (°)	101.827(6)
γ (°)	90
Volume (Å^3)	1922.4(11)
Z	2
Calculated density (g cm^{-3})	1.407
Absorption coefficient (mm^{-1})	1.22
$F(000)$	862
Limiting indices	$-11 \le h \le 11$ $-16 \le k \le 16$ $-20 \le l \le 20$
Reflections collected	16 688
Independent reflections	3769
Data/restraints/parameters	3769/13/238
Goodness-of-fit on F^2	1.13
R indices $[I > 2\sigma(I)]$	$R_1 = 0.0735$ $wR_2 = 0.1991$
R indices (all data)	$R_1 = 0.0999$ $wR_2 = 0.2157$
Largest diff. peak and hole (e Å^{-3})	0.731 to −0.511

TABLE 2 Selected bond lengths (Å) and angles (°) of complex **2**

Cu1–O1	2.064(6)	Cu1–O2	1.907(8)
Cu1–O4	2.792(12)	Cu1–N1	2.194(4)
Cu1–N2	2.042(6)	Cu1–N3	2.069(6)
Cu1–Cl1[a]	2.295(5)		
O1–Cu1–O2	87.3(4)	O1–Cu1–O4	92.6(3)
O1–Cu1–N1	97.5(2)	O1–Cu1–N2	176.9(2)
O1–Cu1–N3	95.6(3)	O2–Cu1–O4	77.7(4)
O2–Cu1–N1	112.0(3)	O2–Cu1–N2	90.1(4)
O2–Cu1–N3	162.8(3)	O4–Cu1–N1	166.2(3)
O4–Cu1–N2	85.1(3)	O4–Cu1–N3	85.2(3)
N1–Cu1–N2	85.1(2)	N1–Cu1–N3	84.5(2)
N2–Cu1–N3	86.4(3)	O1–Cu1–Cl1[a]	77.7(2)
N1–Cu1–Cl1[a]	155.7(2)	N2–Cu1–Cl1[a]	99.2(2)
N3–Cu1–Cl1[a]	119.6(2)		

[a]The minor part of the molecule.

2.8 | Synthesis of Cu(II) Complexes

2.8.1 | $[Cu_2(pxdmbtacn)Cl_4]$ (1)

A methanol solution (5 ml) of $CuCl_2{\cdot}2H_2O$ (0.20 mmol, 0.0341 g) was mixed with a methanol solution (5 ml) of pxdmbtacn (0.10 mmol, 0.0416 g) with stirring. Then the mixture was stirred for a further 2 h under reflux to give a clear blue solution. The solution was filtered, and the filtrate was allowed to evaporate under room temperature until a green powder was obtained. The solid product was washed several times with ether and dried in air. Yield: 0.051 g (74% based on metal precursor). FT-IR (KBr, cm^{-1}): 3517(s), 3434(s), 2923(m), 2866(m), 2823(m), 1598(s), 1457(m), 1345(m), 1215(w), 1158(w), 1069(m), 1002(m), 862(m), 787(m), 702(m), 526(m), 507(m), 424(m). ESI-MS: m/z = 307.1 $[Cu_2(pxdmbtacn)Cl_2]^{2+}$.

2.8.2 | $[Cu_2(pxdmbtacn)Cl_{0.7}(NO_3)_{1.3}(OH)_2(H_2O)_{1.3}]{\cdot}6H_2O$ (2)

Upon mixing $CuCl_2{\cdot}2H_2O$ (0.20 mmol, 0.0341 g) and pxdmbtacn (0.10 mmol, 0.0416 g) in a mixture of methanol (5 ml) and water (5 ml), aqueous NaOH (2 M) was added to adjust the pH of the mixture to 7.0. The reaction mixture was stirred for a further 3 h under reflux, followed by the addition of four equivalents of KNO_3. The solution was filtered and left to evaporate under ambient conditions. Blue plate-shaped single crystals suitable for X-ray analysis were grown within two weeks. Yield: 0.048 g (61% based on metal precursor). FT-IR (KBr, cm^{-1}): 3448(s), 2929(m), 2874(m), 1635(m), 1384(s), 1158(w), 1126(w), 1062(m), 998(m), 901(w), 826(m), 792(m), 744(m), 626(w), 579(w), 541(w), 464(w), 426(w). ESI-MS: m/z = 703.2 $[Cu_2(pxdmbtacn)(NO_3)_2Cl]^+$, 728.2 $[Cu_2(pxdmbtacn)(NO_3)_3]^+$.

2.8.3 | $[Cu_2(pxdiprbtacn)Cl_4]$ (3)

A methanolic solution (5 ml) of $CuCl_2{\cdot}2H_2O$ (0.20 mmol, 0.0341 g) was added dropwise to a methanol solution (5 ml) of pxdiprbtacn (0.10 mmol, 0.0528 g). The resulting reaction mixture was kept at reflux for 3 h with stirring. After cooling, the solution was left at room temperature for slow evaporation and a green powder was precipitated after one day. The solid product was filtered off, washed several times with ether and dried in air. Yield: 0.062 g (78% based on metal precursor). FT-IR (KBr, cm^{-1}): 3437(s), 2970(m), 2835(m), 1639(m), 1489(m), 1446(m), 1385(m), 1294(w), 1215(w), 1140(m), 1099(m), 1075(m), 1015(m), 983(m), 949(w), 865(w), 786(m), 731(m), 622(m), 526(m), 438(w). ESI-MS: m/z = 363.1 $[Cu_2(pxdiprbtacn)Cl_2]^{2+}$, 761.3 $[Cu_2(pxdiprbtacn)Cl_3]^+$.

2.8.4 | $[Cu_2(pxbtacn)Cl_4]$ (4)

The complex was prepared from $CuCl_2{\cdot}2H_2O$ (0.20 mmol, 0.0341 g) and pxbtacn (0.10 mmol, 0.0360 g) following a reported procedure.[57] Yield: 0.054 g (86% based on metal precursor). FT-IR (KBr, cm^{-1}): 3456(s), 3267(s), 2933(m), 2848(m), 1631(m), 1489(m), 1453(m), 1377(m), 1348(m), 1283(m), 1235(w), 1150(w), 1096(m), 1004(s), 943(m), 893(m), 863(m), 827(m), 766(m), 731(m), 628(m), 581(m), 493(w), 428(w). ESI-MS: m/z = 521.1 $[Cu_2(pxdtacn\text{-}2H)Cl]^+$, 593.1 $[Cu_2(pxdtacn)Cl_3]^+$, 1223.1 $[Cu_4(pxdtacn)_2Cl_7]^+$. The phase purity of the as-prepared product was confirmed by the good match of its experimental PXRD pattern with that simulated from the reported crystal structure (Figure S1).

3 | RESULTS AND DISCUSSION

3.1 | Synthesis

The powder products of three chloride complexes were prepared by treating $CuCl_2{\cdot}2H_2O$ and bis-tacn ligands in methanol using a molar ratio of 2:1. Unfortunately, no single crystals of these complexes suitable for X-ray structural analysis could be successfully grown by evaporating their methanolic solutions in air. In order to facilitate the crystallization of dinuclear Cu(II) complexes, four equivalents of KNO_3 were introduced into the solutions of three chloride complexes separately and only blue plate crystals of complex **2** containing partially occupied chloride and nitrate groups were separated from the mother liquid. The physical properties and elemental analysis data for

three bis-tacn ligands and their dinuclear Cu(II) complexes are presented in Table 3.

3.2 | Crystal Structure of Complex 2

Single crystals of complex **2** belong to the monoclinic system, space group $P2_1/n$. The asymmetric unit of the complex is composed of one half of a dinuclear unit and three crystallization water molecules. As depicted in Figure 2, each of the two Cu(II) ions is facially coordinated with three nitrogen atoms (N1, N2 and N3) from tacn backbone and the remaining binding sites around Cu(II) are completed by one hydroxide ion (O1) together with one or more other labile ligand/ligands (either an aqua ligand (O2) and a nitrate ion or a chloride group (Cl1) with an occupancy ratio of 0.65:0.35). When a hydroxide ion, a water molecule and a nitrate ion reside at the labile sites, the coordination geometry around Cu(II) can be regarded as axially elongated octahedral in which the basal plane is defined by two methyl-substituted tacn nitrogen atoms as well as two oxygen atoms provided by both hydroxide and aqua ligands. A tacn nitrogen atom connected to a bulky *p*-xylylene group and a weakly bound nitrate ion occupy the two apical positions. The bond lengths between central Cu(II) and apically coordinated N1 and O4 atoms are 2.194(6) and 2.792(6) Å, respectively. Compared with them, the basal bond distances are much shorter with an average value of 2.021 Å. Except for the markedly larger Cu—O (nitrate) bond length, other corresponding Cu—N and Cu—O bond lengths fall in the normal range expected for octahedral Cu(II) complexes with tacn ligands.[58,59] The *cis* and *trans* bond angles about the Cu(II) center range from 77.7(4)° to 112.0(3)° and from 162.8(3)° to 176.9(2)°, respectively. Some bond angles deviate significantly from the ideal octahedral angles of 90° and 180°, revealing the moderate distortion of the Cu(II) sphere. While a chloride group acts as the labile ligand bound at Cu(II) in place of a water molecule and a nitrate, the geometry about Cu(II) is thus distorted square pyramidal with one chloride group occupying the basal plane. The Cu1—Cl1 bond length of 2.295(5) Å is normal for such a bond in bis-tacn complexes[60,61] but longer than those of other bonds around Cu(II). The whole dinuclear unit is centrosymmetric with the inversion center at the midpoint of the *p*-xylylene spacer. Due to the *anti* conformation assumed by the ditopic ligand pxdmbtacn, two Cu(II) ions within a dinuclear entity are separated from each other by a distance of 11.741 Å, which is close to the Cu···Cu separation of 11.81 Å found in the structure of $[Cu_2(pxbtacn)Cl_4]$.[57]

3.3 | ESR Spectroscopy and Magnetic Properties

The ESR spectrum and magnetic properties of complex **4** have been thoroughly investigated by Spiccia and coworkers,[57] and thus these magnetic characterizations were only conducted for complexes **1** and **3**. The solid-state X-band ESR spectra of complexes **1** and **3** recorded at room temperature are shown in Figure 3. Both spectra exhibit two broad signals in the $\Delta M_s = \pm 1$ region and no half-field transition could be detected at *ca* 1600 G. The analysis of the resonance spectra yields the following ESR parameters: $g_{||} = 2.183$, $g_{\perp} = 2.077$ and $g_{||} = 2.189$, $g_{\perp} = 2.091$ for **1** and **3**, respectively. These spectra are of axial type ($g_{||} > g_{\perp} > 2.0023$) with the unpaired electron localized mainly in the $d_{x^2-y^2}$ orbital of Cu(II) in square pyramidal geometry. The observed $g_{||}$ values for the two complexes are less than 2.3, in agreement with the covalent character of the metal–ligand bonds.[62]

Magnetic susceptibility measurements were performed for complexes **1** and **3** using powdered samples in the temperature range 2–300 K. The magnetic behaviors in the form of χ_m and $\chi_m T$ versus T plots are shown in Figure 4. The observed $\chi_m T$ value of **1** at 300 K is 0.905 cm^3 K mol^{-1}, which is larger than the theoretical spin-only value of 0.75 cm^3 K mol^{-1} expected for two

TABLE 3 Physical properties and elemental analysis of three bis-tacn ligands and their dinuclear Cu(II) complexes

Compound	Formula	Yield (%)	Color	μ_{eff} (BM)	Calcd (found) C (%)	H (%)	N (%)
pxdmbtacn	$C_{24}H_{44}N_6$	86%	Yellow	—	69.23 (69.15)	10.58 (10.63)	20.19 (20.64)
pxdiprbtacn	$C_{32}H_{60}N_6$	74%	Yellow	—	72.67 (72.64)	11.44 (11.40)	15.89 (15.95)
pxbtacn	$C_{20}H_{36}N_6$	62%	Yellow	—	66.63 (66.87)	10.06 (10.34)	23.31 (23.16)
1	$C_{24}H_{44}Cl_4Cu_2N_6$	74%	Green	2.69	42.05 (41.95)	6.47 (6.79)	12.26 (12.03)
2	$C_{24}H_{60.59}Cl_{0.70}Cu_2N_{7.30}O_{13.18}$	61%	Blue	—	35.40 (35.32)	7.50 (7.41)	12.56 (12.49)
3	$C_{32}H_{60}Cl_4Cu_2N_6$	78%	Green	2.59	48.18 (48.18)	7.58 (7.46)	10.53 (10.61)
4	$C_{20}H_{36}Cl_4Cu_2N_6$	86%	Green	2.47	38.16 (38.49)	5.76 (5.91)	13.35 (13.18)

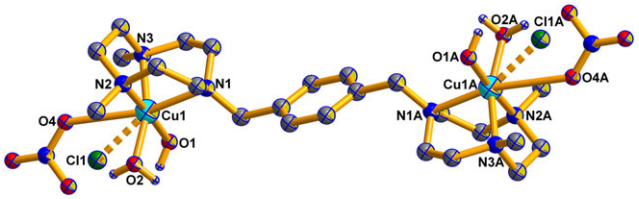

FIGURE 2 Coordination environments of Cu(II) atoms in complex **2**. All hydrogen atoms except those on the coordinated hydroxide groups and water molecules are omitted for clarity. The dashed lines represent the minor part of the disordered components (symmetry code: A $1-x, 1-y, 2-z$)

uncoupled $S = 1/2$ Cu(II) ions. As the temperature is lowered, the $\chi_m T$ value decreases smoothly above 14 K and then drops abruptly to 0.223 cm^3 K mol^{-1} at 2 K. Such a behavior indicates the existence of an antiferromagnetic coupling in **1**. Similar magnetic behavior was also observed for **3**. Its $\chi_m T$ value is 0.837 cm^3 K mol^{-1} at room temperature and decreases to a minimum value of 0.205 cm^3 K mol^{-1} at 2 K. The magnetic susceptibility data for both complexes were fitted by a modified Bleaney–Bowers equation including a correction term for paramagnetic impurity[63] based on the spin Hamiltonian $H = -2JS_1S_2$:

$$\chi_m = \left(2Ng^2\beta^2\right)(1-\rho)/kT[3 + \exp(-2J/kT)] + \left(Ng^2\beta^2\right)\rho/2kT + \text{TIP} \quad (1)$$

where N, g, β, k and T have their usual meanings, $2J$ is the coupling constant between two Cu(II) ions, ρ is the molar fraction of monomeric impurity and TIP denotes the temperature-independent paramagnetism. The best fit of the $\chi_m T$ data led to $g = 2.11$, $2J = -5.20$ cm^{-1}, $\rho = 0.17$, TIP $= 2.68 \times 10^{-4}$ cm^3 mol^{-1} for **1** and $g = 2.06$, $2J = -7.40$ cm^{-1}, $\rho = 0.17$, TIP $= 1.83 \times 10^{-4}$ cm^3 mol^{-1} for **3**.

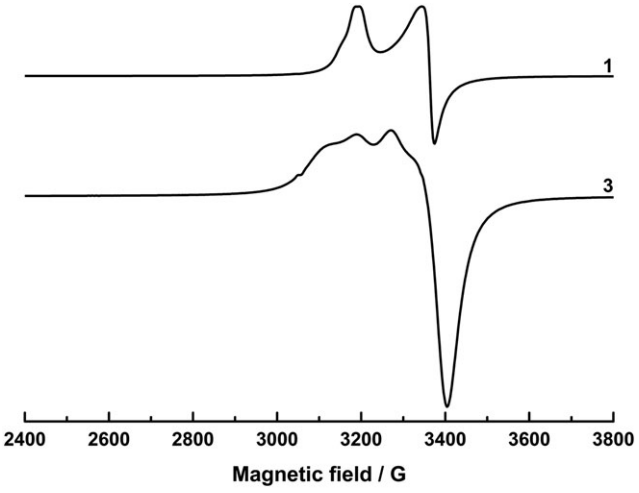

FIGURE 3 X-band ESR spectra of powdered samples of complexes **1** and **3** measured at room temperature

The obtained values for each complex compare well with those reported for complex **4**.[57] The magnetic coupling seems impossible to be transferred intramolecularly across the long *p*-xylylene spacer but more likely to be mediated intermolecularly via a hydrogen bonding pathway between neighboring molecules.

3.4 | FT-IR Spectra

The FT-IR spectra of three bis-tacn ligands and their dinuclear Cu(II) complexes are shown in Figure S2 and some significant absorption bands are listed in Table 4, where the characteristic vibrations of the ligands before and after complexation are compared. The medium intensity bands observed for the free ligands at 1079–1113 cm^{-1} can be assigned to ν(C—N) stretching. In the spectra of the complexes, these bands are shifted towards the lower wavenumber side by about 10–20 cm^{-1}, showing the coordination of the ligands to Cu(II) ions occurs through the macrocyclic nitrogen donors. This is further supported by the appearance of new bands at 424–438 cm^{-1}, which can be attributed to ν(M—N) vibrations.[64] For the free

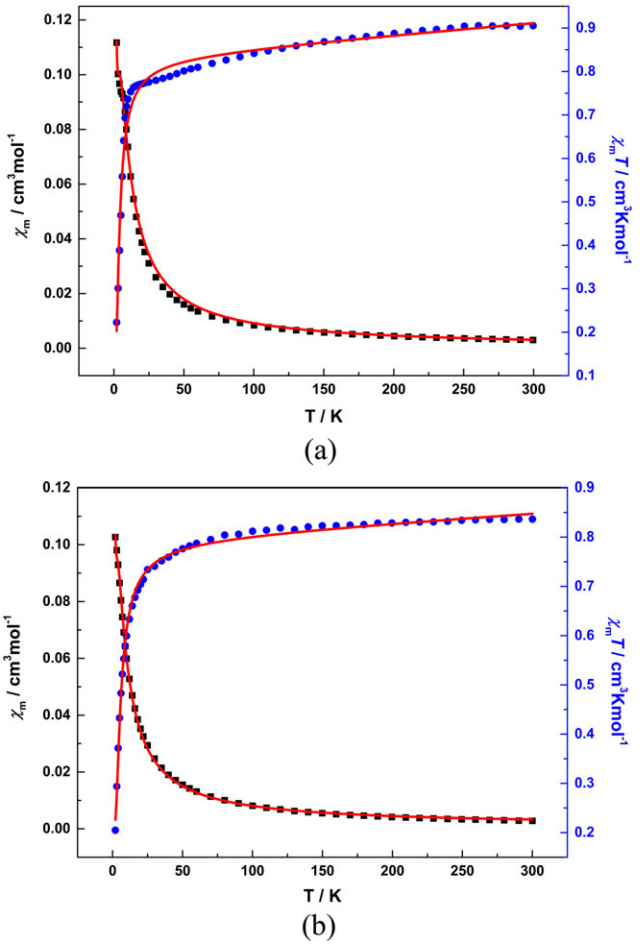

FIGURE 4 Plots of χ_m (■) and $\chi_m T$ (•) versus T for complexes **1** (a) and **3** (b), where the solid lines represent the fitted data

TABLE 4 Significant absorption peaks in the FT-IR spectra of three bis-tacn ligands and their dinuclear Cu(II) complexes[a]

Compound	ν(N—H)	δ(N—H)	$\nu(NO_3)$	ν(C—N)	ν(M—O)	ν(M—N)
pxdmbtacn				1079m		
pxdiprbtacn				1086m		
pxbtacn	3290b	1492m		1113m		
1				1069m		424m
2			1384s	1062m	541w	426w
3				1075m		438w
4	3267s	1489m		1096m		428w

[a]b, broad; s, strong; m, medium; w, weak.

ligand pxbtacn, the characteristic absorption bands at 3290 and 1490 cm^{-1}, due to the N—H stretching and bending vibrations of the secondary amine groups, respectively, are shifted to 3267 and 1489 cm^{-1} in the spectrum of its complex. This observation also indicates the involvement of the macrocyclic nitrogen atoms in coordination. The presence of nitrate ion in **2** is evidenced by a strong peak centered at 1384 cm^{-1}; meanwhile the observation of ν(M—O) band at 541 cm^{-1} confirms the binding of H_2O/OH^- group to the central Cu(II) ions in this complex.[65]

3.5 | UV–Visible Spectra

By examining the solid-state UV–visible spectra of the three dinuclear Cu(II) complexes **1**, **3** and **4** with those of their respective ligands (Figure 5), a medium strong absorption band is observed in the spectral region from 240 to 400 nm for each of the three complexes (277, 271 and 258 nm for **1**, **3** and **4**, respectively) but which is not conspicuous in the spectra of the respective ligands. Thus, this band is interpreted as the ligand-to-metal charge transfer process from either the chloride or the macrocyclic nitrogen donors to the square pyramidal Cu(II) ion. The characteristic d–d transition of the central d^9 Cu(II) ion, as expected, emerges at 675, 711 and 657 nm for **1**, **3** and **4**, respectively. The UV–visible spectra of complexes **1** and **3** recorded in water are similar to their solid-state spectra although the ligand-to-metal charge transfer band and the Cu(II) d–d transition are separately shifted to longer wavelengths (288 and 298 nm for **1** and **3**, respectively) and shorter wavelengths (632 and 660 nm for **1** and **3**, respectively). However, on dissolving in water the two bands of **4** are blue-shifted to 252 and 639 nm, respectively. The shift of the electronic absorption bands can probably be ascribed to the different coordination environment of Cu(II) in aqueous solution compared to the solid state, which results from the substitution of chloride bound to Cu(II) by other small ligands such as water or hydroxide ion.

Since the biological activities of the metal complexes are strongly dependent on their existing forms in solution, the solution stability of complexes **1** and **3** in phosphate buffer at pH = 7.4 was evaluated using UV–visible spectroscopy. As depicted in Figure S3, within a 48 h period, the intensity of the d–d transition band of Cu(II) for both complexes decreases slightly and no shift of the absorption maximum occurs, providing evidence that for these complexes the coordination sphere around central Cu(II) remains intact in the neutral buffer medium. Furthermore, the stability of complex **3** in alkaline solution was determined by monitoring its UV–visible spectra in the pH range from 7 to 12. With the increase of basicity, the absorption band due to the d–d transition of Cu(II) undergoes a minor hypsochromic shift from 652 to 641 nm accompanied by an irregular change of the band intensity. The slight change of the metal-centered band implies that there are no significant structural and electronic properties changes in Cu(II) centers. Therefore, it is expected that the complex can still exist in alkaline solution as a dinuclear species although the removable small molecules around Cu(II) might be varied. This

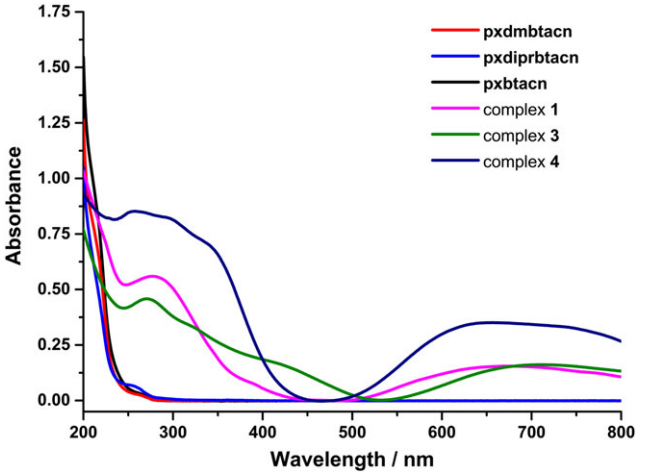

FIGURE 5 Solid-state UV–visible absorption spectra of complexes **1**, **3** and **4** and their respective ligands

conclusion was further confirmed by the mass spectrometric analysis.

3.6 | ESI-MS Analysis

ESI-MS was used to investigate the structural stability of the dinuclear motif of complexes **1**, **3** and **4** in their aqueous solutions. Only one major peak at m/z = 307.09 (100%) is observed in the positive-ion mode ESI-MS spectrum of complex **1**, which can be assigned to the dication $[Cu_2(pxdmbtacn)Cl_2]^{2+}$. The mass spectrum of **2** shows two major singly charged ions $[Cu_2(pxdmbtacn)(NO_3)_2Cl]^+$ and $[Cu_2(pxdmbtacn)(NO_3)_3]^+$ at m/z = 703.17 (100%) and 728.17 (79%), respectively. Complex **3** dissolved in water exhibits two dominant peaks at m/z = 363.14 (100%) and 761.25 (34%), which correspond to the dinuclear fragment ions $[Cu_2(pxdiprbtacn)Cl_2]^{2+}$ and $[Cu_2(pxdiprbtacn)Cl_3]^+$, respectively. When the pH of this solution was adjusted to 10 by adding aqueous NaOH, both peaks disappear and new signals are seen at m/z = 410.15 (100%) and 797.35 (49%). These peaks can be attributed to the doubly charged ions $[Na_2Cu_2(pxdiprbtacn))(CO_3)_2]^{2+}$ and $[NaCu_2(pxdiprbtacn))(CO_3)_2]^+$ each containing two CO_3^{2-} anions, where one CO_3^{2-} ion is in place of two chloride anions and involved in chelation to one central Cu(II) ion. The source of CO_3^{2-} may be tentatively ascribed to capture of atmospheric CO_2 by the alkaline solution. The experimental isotopic distribution patterns of these peaks match well with the calculated ones. For complex **4**, four monocationic peaks are observed in the m/z range 500–800 with the dominant peak centered at m/z = 593.06 (100%) being the dinuclear cation $[Cu_2(pxbtacn)Cl_3]^+$. One further peak with lower intensity due to the dimeric species $[Cu_4(pxbtacn)_2Cl_7]^+$ can be seen at m/z = 1223.09 (64%). The result indicates that **4** may partially dimerize into a tetranuclear species in aqueous solution in addition to existing as a dinuclear molecule. The mass spectra of complexes **1**, **3** and **4** are presented in Figure S4 and the insets show the experimental and calculated isotopic distribution patterns of some major ions in the respective spectra.

3.7 | Cyclic Voltammetry

The redox behavior of complexes **1** and **3** was investigated via cyclic voltammetry in a three-electrode system equipped with saturated Ag/AgCl reference electrode. Figure S5 shows the representative voltammograms of two complexes in aqueous solution at room temperature. The cyclic voltammetry curve of **1** reveals two reduction waves with $E_{1/2}$ of 0.659 and −0.862 V versus Ag/AgCl electrode during the cathodic scan from 2.0 to −1.0 V. The ratio of the peak currents deviates from unity and the peak-to-peak separations are larger than 300 mV, indicative of the irreversibility of these two redox processes. Complex **3** undergoes two stepwise reductions in the potential range from 1.6 to −0.8 V. The first wave with $E_{1/2}$ of 0.218 V (versus Ag/AgCl) seems to be quasi-reversible with a separation between the potential peaks of 171 mV, whereas the second one with $E_{1/2}$ of −0.283 V (versus Ag/AgCl) is characteristic of an irreversible electrochemical process since the peak-to-peak separation approaches 400 mV. The determined redox potentials for these two Cu(II) complexes compare well with those found for other dinuclear Cu(II) complexes.[66] The observed two redox processes might be attributed to the successive one-electron transfer reduction of the dinuclear Cu(II) moieties given in the form of equations 2 and 3:

$$Cu^{II}Cu^{II} + e^- \rightarrow Cu^{II}Cu^{I} \quad (2)$$

$$Cu^{II}Cu^{I} + e^- \rightarrow Cu^{I}Cu^{I} \quad (3)$$

Since at least one of the half-wave potentials of the two redox processes for complexes **1** and **3** lies between the reduction potentials corresponding to $O_2/O_2^{\bullet-}$ (+0.02 V versus Ag/AgCl) and $O_2^{\bullet-}/H_2O_2$ (+1.11 V versus Ag/AgCl) redox couples in neutral solution, these complexes are considered to be competent SOD mimicking systems capable of cleaning the superoxide radical.[10]

3.8 | DNA Cleavage

The chemical nuclease activities of complexes **1** and **3** towards supercoiled pBR322 DNA were investigated by gel electrophoresis in the absence and presence of H_2O_2 under near-physiological conditions (pH = 6.8). Although complex **4** cannot exist merely as dinuclear species in aqueous solution, for a comparison the plasmid DNA scission activity of complex **4** in HEPES buffer solution was also evaluated, with its initial concentration and other experimental conditions being identical to those used in the assays for other two complexes. The DNA cleavage efficiency was assessed by determining the ability of these complexes to convert the plasmid DNA from the original supercoiled form (Form I) to the open circular (nicked) form (Form II) and the linear form (Form III).

The extent of cleavage for pBR322 DNA in the presence of the three complexes without the redox agent could be ignorable, which indicates that all three complexes do not exhibit detectable nuclease activity towards

supercoiled DNA individually. Due to the redox activity of Cu(II) ion, most of the reported Cu(II)-based DNA cleavage agents act via an oxidative mechanism. In the oxidative degradation of plasmid DNA, H_2O_2 is commonly used as a reducing reagent to generate ROS, i.e. hydroxyl radical, singlet oxygen, superoxide anion as well as reactive metal–oxo adducts, under the mediation of Cu(II) complexes. One or more of them is/are responsible for the subsequent chemical cleavage of the supercoiled plasmid DNA. Given those finding, the nuclease activities of the three Cu(II) complexes were assayed with the aid of H_2O_2. As shown in Figure 6, complexes **1** and **3** can effectively cleave supercoiled pBR322 DNA to open circular and linear forms even if their concentrations are as low as 1 μM, but the cleavage of DNA by **4** only can be observed when its concentration is higher than 2 μM. The supercoiled DNA (Form I) can almost be completely converted into degraded forms catalyzed by one of the three complexes at a concentration of 8, 16 and 20 μM for **1**, **3** and **4**, respectively. Meanwhile linear DNA (Form III) begins to appear when the concentration of **1** is 6 μM and also as it is raised to 12 and 20 μM for **3** and **4**, respectively. It is evident that complex **1** exhibits higher nuclease efficiency than **3** and **4**. Furthermore, the plasmid DNA cleavage processes mediated by the three complexes are all concentration-dependent ones.

To determine which ROS is responsible for the oxidative degradation of plasmid DNA in the H_2O_2-containing cleavage systems discussed above, various ROS scavengers,[67] namely diffusible hydroxyl radical scavengers (DMSO and ethanol), singlet oxygen scavengers (L-histidine and NaN_3), superoxide scavenger (SOD) and H_2O_2 scavenger (KI), were introduced into the reaction systems before the addition of the said complexes under the same cleavage conditions. As can be seen in Figure 7, the cleavage activity of all complexes is inhibited markedly in the presence of H_2O_2 scavenger (KI), making clear the crucial role of H_2O_2 in such oxidative cleavage. Addition of L-histidine into the cleavage system also inhibits the DNA cleavage to some degree for all catalysts, evidencing the possibility that singlet oxygen species may be involved in the cleavage process. For **1** and **4**, the superoxide

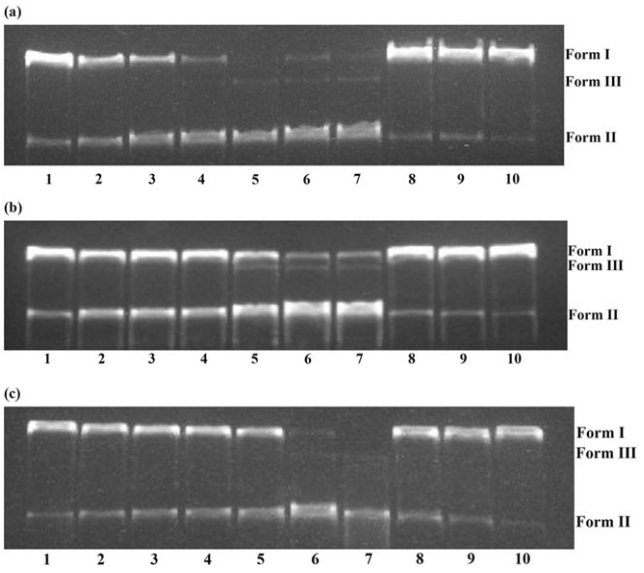

FIGURE 6 Cleavage of pBR322 DNA mediated by complexes **1** (a), **3** (b) and **4** (c) at various concentrations in HEPES buffer after 2 h incubation at 37 °C. (a) Lanes 1–7: DNA + 0.50 mM H_2O_2 + **1** ([**1**] = 1, 2, 4, 6, 8, 10 and 12 μM); lane 8: DNA + 0.50 mM H_2O_2 + 12 μM $CuCl_2$; lane 9: DNA + 0.50 mM H_2O_2 + 12 μM pxdmbtacn; lane 10: DNA control. (b) Lanes 1–7: DNA + 0.50 mM H_2O_2 + **3** ([**3**] = 1, 2, 4, 8, 12, 16 and 20 μM); lane 8: DNA + 0.50 mM H_2O_2 + 20 μM $CuCl_2$; lane 9: DNA + 0.50 mM H_2O_2 + 20 μM pxdiprbtacn; lane 10: DNA control. (c) Lanes 1–7: DNA + 0.50 mM H_2O_2 + **4** ([**4**] = 2, 4, 8, 12, 16, 20 and 24 μM); lane 8: DNA + 0.50 mM H_2O_2 + 24 μM $CuCl_2$; lane 9: DNA + 0.50 mM H_2O_2 + 24 μM pxbtacn; lane 10: DNA control

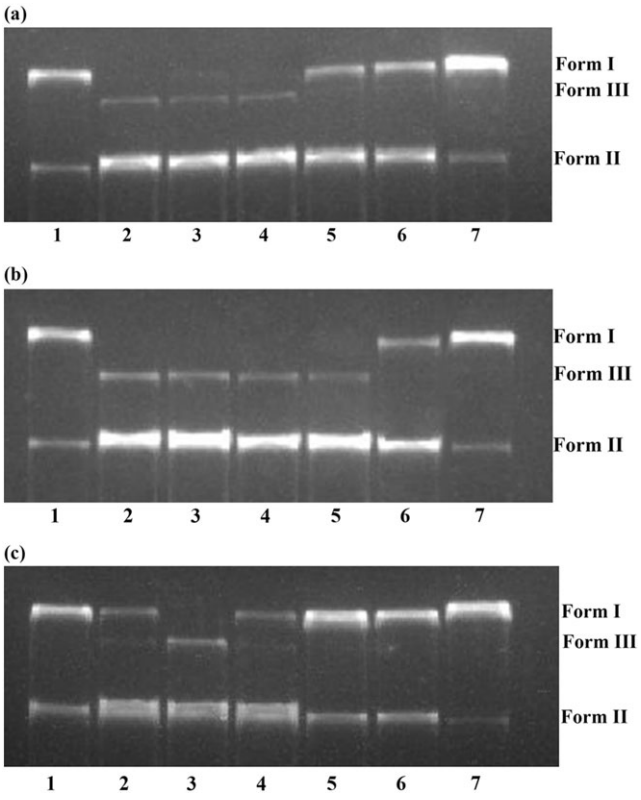

FIGURE 7 Cleavage of pBR322 DNA by 20 μM of complexes **1** (a), **3** (b) and **4** (c) and different inhibitors in HEPES buffer after 2 h incubation at 37 °C. (a) Lanes 1–6: DNA + 0.50 mM H_2O_2 + **1** + different inhibitors (1 mM KI, 1 mM C_2H_5OH, 1 mM NaN_3, 1 mM DMSO, 20 U ml^{-1} SOD and 1 mM L-histidine); lane 7: DNA control. (b) Lanes 1–6: DNA + 0.50 mM H_2O_2 + **3** + different inhibitors (1 mM KI, 1 mM C_2H_5OH, 1 mM NaN_3, 1 mM DMSO, 20 U ml^{-1} SOD and 1 mM L-histidine); lane 7: DNA control. (c) Lanes 1–6: DNA + 0.50 mM H_2O_2 + **4** + different inhibitors (1 mM KI, 1 mM C_2H_5OH, 1 mM NaN_3, 1 mM DMSO, 20 U ml^{-1} SOD and 1 mM L-histidine); lane 7: DNA control

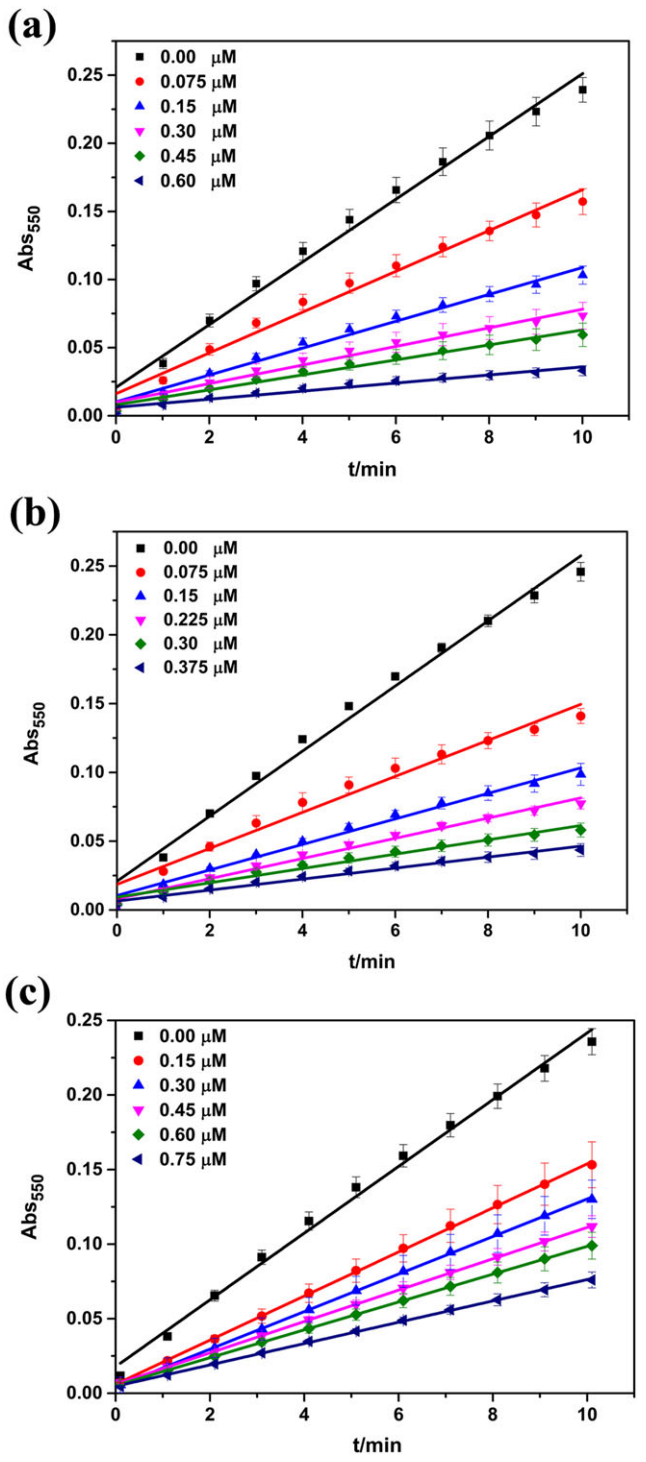

FIGURE 8 Absorbance values (Abs_{550}) as a function of time plotted for varying concentrations of complexes **1** (a), **3** (b) and **4** (c)

scavenger (SOD) also prevents the DNA degradation partially; thus the involvement of superoxide anion could not be ruled out for the oxidative cleavage system containing **1** or **4**. From these results, we can concluded that the DNA cleavage mediated by these complexes may follow an oxidative mechanism in which reactive Cu(I) species deriving from the Cu(II) precursors is likely favorable for the generation of ROS.

3.9 | SOD-Like Activity

The SOD activities of the three Cu(II) complexes were measured following an indirect method by utilizing NBT as a superoxide anion indicator,[68] which is based on the kinetic competition between the mimic and NBT for reacting with $O_2^{\bullet-}$. In this indirect method, SOD activity is inversely related to the amount of formazan formed by the reaction of superoxide anion with NBT, which is spectrally detected at 550 nm. The reduction of NBT was examined after the introduction of each of the three Cu(II) complexes to the reaction system under physiological conditions (pH = 7.4) and the plots of absorbance at 550 nm against time in the presence of varying concentrations of Cu(II) complexes are shown in Figure 8. The inhibition percentage of NBT reduction was determined spectrophotometrically for each complex and the catalytic activity was evaluated by the inhibitor concentration for 50% inhibition of NBT reduction (IC_{50}) (Figure 9). It is clear that complexes **1**, **3** and **4** can efficaciously inhibit the reduction of NBT at physiological pH and the SOD-like activities of these Cu(II) complexes are found to decrease in the order: **3** > **1** > **4**. The IC_{50} values of the three mimic complexes are summarized in Table 5 and compared to those of native CuZnSOD, and some azamacrocyclic mononuclear and dinuclear Cu(II) compounds reported in the literature. It can be seen that the first two complexes described in the present work are among the most active Cu(II) mimic compounds known. Their remarkable SOD-like activities may be ascribed to the convenient substitution of labile Cl^- or other small ligands bound at Cu(II) active sites by the substrate $O_2^{\bullet-}$ during the catalytic process. The SOD-like activity of **4** is about 3–4 times lower than those of complexes **1** and **3**. The lower activity of **4** is due to the fact that the complex

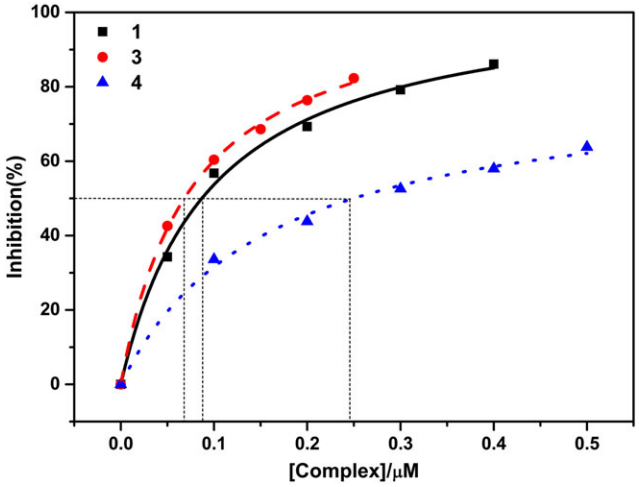

FIGURE 9 Inhibition percentage of NBT reduction with increasing concentration of complexes **1**, **3** and **4**

TABLE 5 SOD-like activities of complexes **1**, **3** and **4**, native CuZnSOD and some reported azamacrocyclic Cu(II) model complexes[a]

System	IC_{50} (μM)	Experimental method	Ref.
1	0.087	McCord–Fridovich (NBT)	This work
3	0.068	McCord–Fridovich (NBT)	This work
4	0.25	McCord–Fridovich (NBT)	This work
Native CuZnSOD	0.015	McCord–Fridovich (NBT)	This work
$[Cu(L^1)Cl]ClO_4$	0.90	Riboflavin (NBT)	[39]
$[Cu(L^2)CH_3CN](ClO_4)_2{\cdot}H_2OClO_4$	0.76	Riboflavin (NBT)	[39]
$[CuCl(L^3)]{\cdot}PF_6{\cdot}EtOH$	0.32	Riboflavin (NBT)	[43]
$[Cu(L^4)]{\cdot}(ClO_4)_2{\cdot}CH_3CH_2OH$	3.3	Riboflavin (NBT)	[47]
$[Cu_2HL^5Br_2](ClO_4)_3{\cdot}1.5H_2O$	2.93	McCord–Fridovich (NBT)	[69]
$[(CuimCu)L^6]ClO_4{\cdot}0.5H_2O$	0.62	McCord–Fridovich (NBT)	[70]
Cu_2L^7	0.11	McCord–Fridovich (NBT)	[71]
$[Cu_2L^8(im)](ClO_4)_3{\cdot}4H_2O$	1.96	Riboflavin (NBT)	[72]

[a]L^1 = 1-(benzimidazole-2-ylmethyl)-1,4,7-triazacyclononane, L^2 = 1,4-bis(benzimidazole-2-ylmethyl)-1,4,7-triazacyclononane, L^3 = 1-carboxylic acid ethyl ester-4,7-bis(*R*)-1,4,7-triazacyclononane, L^4 = 1,2-bis(1,4,7-triazacyclonon-1-yl)ethane, L^5 = 6-[6′-[3,6,9-triaza-1-(2,6-pyridina)cyclodecaphan-6-yl]-3-azahexyl]-3,6,9-triaza-1-(2,6-pyridina)cyclodecaphane, L^6 = 3,6,9,16,19,22-hexaaza-6,19-bis(2-hydroxyethyl)tricyclo[22,2,2,211,14]triaconta-1,11,13,24,27,29-hexaene, L^7 = 3,7,11,15,19,23-hexaaza-1(2,6)-pyridinacyclotetracosaphane, L^8 = 3,6,9,16,19,22-hexaaza-6,19-bis(1*H*-imidazol-4-ylmethyl)tricyclo[22,2,2,2,11,14]triaconta-1,11,13,24,27,29-hexaene.

is subject to dimerization in solution, and the resultant dimer has fewer labile sites and enhanced steric hindrance at active centers, which is unfavorable for the binding of substrate ($O_2^{\bullet-}$). Since the tertiary amine nitrogen atoms of the bis-tacn ligands present in complexes **1** and **3** are respectively substituted by methyl or isopropyl groups besides xylylene spacer, the dimerization of the dinuclear components can be effectively blocked in their solutions due to the steric substituents.

Considering the much lower molecular weights of complexes **1** and **3** with respect to that of the native CuZnSOD enzyme and the comparable IC_{50} values of 0.087 and 0.068 μM of two complexes with that of the native enzyme (0.015 μM) (relative activity of 16.8 and 21.5% for complexes **1** and **3**, respectively), these two complexes may be regarded as promising SOD mimics.

3.10 | Catalase-Like Activity

H_2O_2 is one of the products during the disproportionation of $O_2^{\bullet-}$ catalyzed by SOD mimics and it also exhibits a deleterious effect on living organisms in relatively higher concentrations. It is more attractive if these mimicking complexes can exhibit both SOD and catalase activities; thus the catalase-like activities of the three complexes

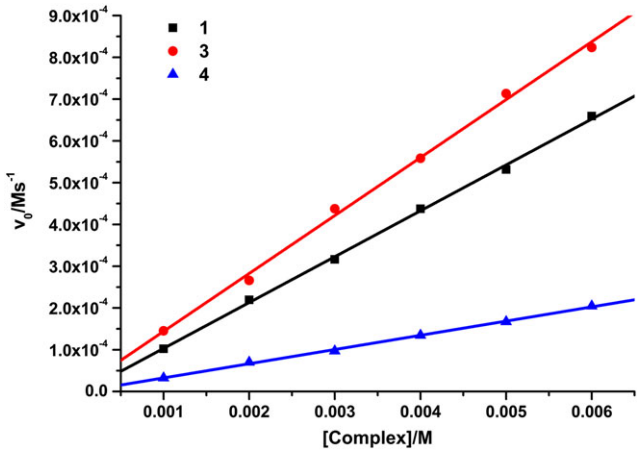

FIGURE 10 Initial rate (v_0) of H_2O_2 dismutation as a function of concentration of complexes **1**, **3** and **4** at a constant concentration of H_2O_2 (200 mM)

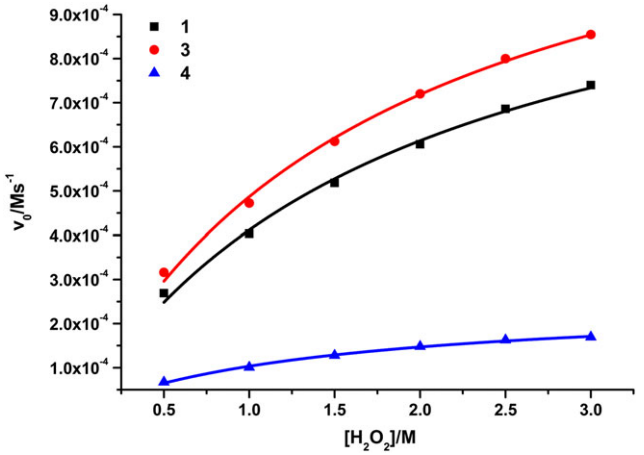

FIGURE 11 Initial rate (v_0) of H_2O_2 dismutation as a function of concentration of H_2O_2 at a constant concentration of complexes **1**, **3** and **4** (2 mM)

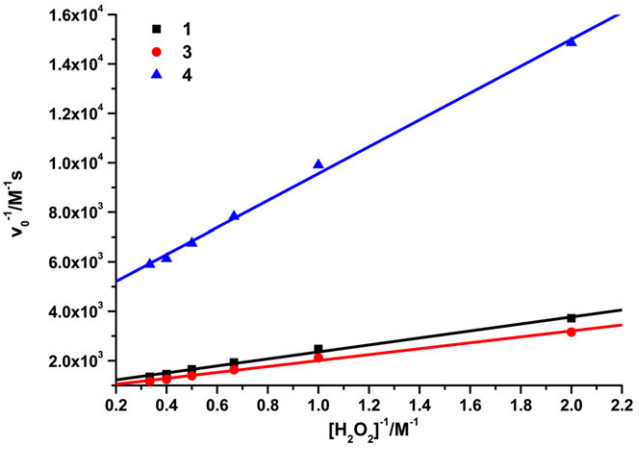

FIGURE 12 Double reciprocal Lineweaver–Burk plots for complexes **1**, **3** and **4**

were investigated in water by volumetric measurement of the evolved oxygen.

At a set of constant concentrations of complex and H_2O_2, the time courses of oxygen evolution in the presence of complexes **1**, **3** and **4** are depicted in Figure S6. Both complexes **1** and **3** show a moderate catalytic activity towards the disproportionation of H_2O_2 but complex **4** is much less active. Again, this can be interpreted by the fact that the partial dimerization of this complex leads to tetranuclear species leaving fewer binding sites for substrates. When the H_2O_2 concentration was kept at 200 mM, the initial rate of H_2O_2 dismutation shows a linear variation with the concentration of all mimic complexes (Figure 10). While at a constant complex concentration of 2 mM, all complexes exhibit saturation kinetics with respect to increasing concentration of H_2O_2, suggesting a Michaelis–Menten-type behavior (Figure 11). The kinetic parameters for H_2O_2 disproportionation were estimated by fitting the experimental data to the Michaelis–Menten equation (Figure 12) and the values of k_{cat}, K_M and k_{cat}/K_M are 1.06 s^{-1}, 1.50 M and 0.71 M^{-1} s^{-1} for **1**, 1.24 s^{-1}, 1.49 M and 0.83 M^{-1} s^{-1} for **3** and 0.24 s^{-1}, 1.32 M and 0.18 M^{-1} s^{-1} for **4**. The catalytic efficiency of complexes **1**, **3** and **4** is higher than those measured for several reported dicopper(II) mimic compounds in the absence of heterocyclic base.[73,74]

4 | CONCLUSIONS

With two *p*-xylylene-bridged bis-tacn ligands bearing pendant alkyl substitutes, two new dinuclear Cu(II) chloride complexes were obtained and their enzyme-like activities were compared to that of a reported Cu(II) complex based on an analogous bis-tacn ligand without pendant group. The steric alkyl groups attached to the macrocyclic skeleton can effectively hinder the dimerization of the dinuclear complexes **1** and **3** whereas complex **4** is able to form a dimeric tetranuclear cluster in aqueous solution. Complexes **1**, **3** and **4** render effective oxidative cleavage of supercoiled plasmid DNA in the presence of H_2O_2. The SOD- and catalase-like activities of complexes **1** and **3** are comparable to that of native CuZnSOD and significantly higher than that of complex **4**. The lower enzymatic activity of complex **4** is derived from the fact that its dimeric species generated in solution has fewer labile coordination sites and increasing steric hindrance around active centers, which are unfavorable for the binding of substrate.

ACKNOWLEDGMENTS

This work was financially supported by the National Natural Science Foundation of China (grant no. 21361004), the Guangxi Natural Science Foundation of China (grant nos. 2014GXNSFAA118044, 2017GXNSFAA198125) and the Natural Science Foundation of Key Laboratory for Chemistry and Molecular Engineering of Medicinal Resources (Guangxi Normal University), Ministry of Education of China (CMEMR2012-A08, CMEMR2013-C08).

ORCID

Zhong Zhang http://orcid.org/0000-0002-8445-0732

REFERENCES

[1] R. S. Balaban, S. Nemoto, T. Finkel, *Cell* **2005**, *120*, 483.

[2] B. Halliwell, *Am. J. Med.* **1991**, *91*, 14S.

[3] I. Fridovich, *J. Biol. Chem.* **1997**, *272*, 18515.

[4] E. Gaggelli, H. Kozlowski, D. Valensin, G. Valensin, *Chem. Rev.* **2006**, *106*, 1995.

[5] M. Hayyan, M. A. Hashim, I. M. Al-Nashef, *Chem. Rev.* **2016**, *116*, 3029.

[6] H. J. Forman, M. Maiorino, F. Ursini, *Biochemistry* **2010**, *49*, 835.

[7] H. Sies, *J. Biol. Chem.* **2014**, *289*, 8735.

[8] A.-F. Miller, *FEBS Lett.* **2012**, *586*, 585.

[9] J. J. P. Perry, D. S. Shin, E. D. Getzoff, J. A. Tainer, *Biochim. Biophys. Acta* **2010**, *1804*, 245.

[10] Y. Sheng, I. A. Abreu, D. E. Cabelli, M. J. Maroney, A.-F. Miller, M. Teixeira, J. S. Valentine, *Chem. Rev.* **2014**, *114*, 3854.

[11] P. Chelikania, I. Fitab, P. C. Loewena, *Cell. Mol. Life Sci.* **2004**, *61*, 192.

[12] A. J. Wu, J. E. Penner-Hahn, V. L. Pecoraro, *Chem. Rev.* **2004**, *104*, 903.

[13] D. Robbins, Y. Zhao, *Antioxid. Redox Signaling* **2014**, *20*, 1628.

[14] A. Bafana, S. Dutt, A. Kumar, S. Kumar, P. S. Ahuja, *J. Mol. Catal. B* **2011**, *68*, 129.

[15] R. A. Greenwald, *Free Radical Biol. Med.* **1990**, *8*, 201.

[16] C. Muscoli, S. Cuzzocrea, D. P. Riley, J. L. Zweier, C. Thiemermann, Z.-Q. Wang, D. Salvemini, *Br. J. Pharmacol.* **2003**, *140*, 445.

[17] H. Sheng, R. E. Chaparro, T. Sasaki, M. Izutsu, R. D. Pearlstein, A. Tovmasyan, D. S. Warner, *Antioxid. Redox Signaling* **2014**, *20*, 2437.

[18] D. P. Riley, *Chem. Rev.* **1999**, *99*, 2573.

[19] R. Krämer, *Angew. Chem. Int. Ed.* **2000**, *39*, 4469.

[20] I. Batinić-Haberle, J. S. Rebouças, I. Spasojević, *Antioxid. Redox Signaling* **2010**, *13*, 877.

[21] S. Signorella, C. Hureau, *Coord. Chem. Rev.* **2012**, *256*, 1229.

[22] B. J. Day, *Biochem. Pharmacol.* **2009**, *77*, 285.

[23] O. Iranzo, *Bioorg. Chem.* **2011**, *39*, 73.

[24] D. Salvemini, Z.-Q. Wang, J. L. Zweier, A. Samouilov, H. Macarthur, T. P. Misko, M. G. Currie, S. Cuzzocrea, J. A. Sikorski, D. P. Riley, *Science* **1999**, *286*, 304.

[25] I. Spasojević, I. Batinić-Haberle, *Inorg. Chim. Acta* **2001**, *317*, 230.

[26] Y. Watanabe, A. Namba, N. Umezawa, M. Kawahata, K. Yamaguchi, T. Higuchi, *Chem. Commun.* **2006**, *4958*.

[27] W.-T. Lee, S. B. Muñoz III, D. A. Dickie, J. M. Smith, *Angew. Chem. Int. Ed.* **2014**, *53*, 9856.

[28] K. D. Mjos, C. Orvig, *Chem. Rev.* **2014**, *114*, 4540.

[29] Z.-Q. Wang, F. Porreca, S. Cuzzocrea, K. Galen, R. Lightfood, E. Masini, C. Muscoli, V. Mollace, M. Ndengele, H. Ischiropoulos, D. J. Salvemini, *Pharmacol. Exp. Ther.* **2004**, *309*, 869.

[30] M. Di Napoli, F. Papa, *IDrugs* **2005**, *8*, 67.

[31] D. P. Riley, O. F. Schall, *Adv. Inorg. Chem.* **2007**, *59*, 233.

[32] T. Joshi, B. Graham, L. Spiccia, *Acc. Chem. Res.* **2015**, *48*, 2366.

[33] J. Qian, S. Yu, W. Wang, L. Wang, J. Tian, S. Yan, *Dalton Trans.* **2014**, *43*, 2646.

[34] J. Qian, X. Ma, J. Tian, W. Gu, J. Shang, X. Liu, S. Yan, *J. Inorg. Biochem.* **2010**, *104*, 993.

[35] Z. Zhang, Z.-R. Geng, X.-W. Kan, Q. Zhao, Y.-Z. Li, Z.-L. Wang, *Inorg. Chim. Acta* **2010**, *363*, 1805.

[36] X. Sheng, X. Guo, X.-M. Lu, G.-Y. Lu, Y. Shao, F. Liu, Q. Xu, *Bioconjugate Chem.* **2008**, *19*, 490.

[37] E. L. Hegg, J. N. Burstyn, *J. Am. Chem. Soc.* **1995**, *117*, 7015.

[38] S. Delagrange, R. Delgado, F. Nepveu, *J. Inorg. Biochem.* **2000**, *81*, 65.

[39] Q.-X. Li, Q.-H. Luo, Y.-Z. Li, M.-C. Shen, *J. Chem. Soc. Dalton Trans.* **2004**, *2329*.

[40] Q.-X. Li, Q.-H. Luo, Y.-Z. Li, Z.-Q. Pan, M.-C. Shen, *Eur. J. Inorg. Chem.* **2004**, *4447*.

[41] Q.-X. Li, Q. Li, R. Chen, X.-L. Yang, J.-Y. Zhou, H.-B. Xu, *Inorg. Chem. Commun.* **2010**, *13*, 1293.

[42] V. R. de Almeida, F. R. Xavier, R. E. H. M. B. Osório, L. M. Bessa, E. L. Schilling, T. G. Costa, T. Bortolotto, A. Cavalett, F. A. V. Castro, F. Vilhena, O. C. Alves, H. Terenzi, E. C. A. Eleutherio, M. D. Pereira, W. Haase, Z. Tomkowicz, B. Szpoganicz, A. J. Bortoluzzia, A. Neves, *Dalton Trans.* **2013**, *42*, 7059.

[43] Q.-X. Li, X. Chen, W.-L. Wang, X.-G. Meng, *J. Coord. Chem.* **2017**, *70*, 1554.

[44] G. B. Shul'pin, G. V. Nizova, Y. N. Kozlov, I. G. Pechenkina, *New J. Chem.* **2002**, *26*, 1238.

[45] T. H. Bennur, D. Srinivas, S. Sivasanker, V. G. Puranik, *J. Mol. Catal. A* **2004**, *219*, 209.

[46] F. Marken, J. E. Taylor, M. J. Bonne, M. E. Helton, M. L. Parry, V. McKee, *Langmuir* **2007**, *23*, 2239.

[47] Q.-X. Li, X.-F. Wang, L. Cai, Q. Li, X.-G. Meng, A.-G. Xuan, S.-Y. Huang, J. Ai, *Inorg. Chem. Commun.* **2009**, *12*, 145.

[48] M. Kose, P. Goring, P. Lucas, V. McKee, *Inorg. Chim. Acta* **2015**, *435*, 232.

[49] R. Kubota, S. Imamura, T. Shimizu, S. Asayama, H. Kawakami, *ACS Med. Chem. Lett.* **2014**, *5*, 639.

[50] M. E. Aliaga, D. Andrade-Acuna, C. Lopez-Alarcon, C. Sandoval-Acuna, H. Speisky, *J. Inorg. Biochem.* **2013**, *129*, 119.

[51] D. Moreno, V. Daier, C. Palopoli, J.-P. Tuchagues, S. Signorella, *J. Inorg. Biochem.* **2010**, *104*, 496.

[52] Z. Liu, G. B. Robinson, E. M. Gregory, *Arch. Biochem. Biophys.* **1994**, *315*, 74.

[53] A. X. S. Bruker, *SAINT Software Reference Manual*, Madison, WI **1998**.

[54] G. M. Sheldrick, *SADABS: Program for Empirical Absorption Correction of Area Detector Data*, University of Göttingen, Germany **1996**.

[55] G. M. Sheldrick, *SHELXTL NT Version 5.1: Program for Solution and Refinement of Crystal Structures*, University of Göttingen, Germany **1997**.

[56] B. Graham, G. D. Fallon, M. T. W. Hearn, D. C. R. Hockless, G. Lazarev, L. Spiccia, *Inorg. Chem.* **1997**, *36*, 6366.

[57] F. H. Fry, L. Spiccia, P. Jensen, B. Moubaraki, K. S. Murray, E. R. T. Tiekink, *Inorg. Chem.* **2003**, *42*, 5594.

[58] A. J. Black, I. A. Fallis, R. O. Gould, S. Parsons, S. A. Ross, M. Schröder, *J. Chem. Soc. Dalton Trans.* **1996**, 4379.

[59] W. Han, L. Li, W. Gu, Z.-Q. Liu, S.-P. Yan, D.-Z. Liao, Z.-H. Jiang, P. Cheng, *J. Coord. Chem.* **2004**, *57*, 41.

[60] X. Zhang, W.-Y. Hsieh, T. N. Margulis, L. J. Zompa, *Inorg. Chem.* **1995**, *34*, 2883.

[61] R. Haidar, M. Ipek, B. DasGupta, M. Yousaf, L. J. Zompa, *Inorg. Chem.* **1997**, *36*, 3125.

[62] D. Kivelson, R. Neiman, *J. Chem. Phys.* **1961**, *35*, 149.

[63] Z. Xu, L. K. Thompson, D. O. Miller, *Inorg. Chem.* **1997**, *36*, 3985.

[64] K. Nakamoto, *Infrared and Raman Spectra of Inorganic and Coordination Compounds, Part B: Applications in Coordination, Organometallic, and Bioinorganic Chemistry*, 5th ed., Wiley-Interscience, New York **1997**.

[65] B. Dede, İ. Özmen, F. Karipcin, M. Cengiz, *Appl. Organometal. Chem.* **2009**, *23*, 512.

[66] R. N. Patel, Y. P. Singh, Y. Singh, R. J. Butcher, J. P. Jasinski, *Polyhedron* **2017**, *129*, 164.

[67] S. Poornima, K. Gunasekaran, M. Kandaswamy, *Dalton Trans.* **2015**, *44*, 16361.

[68] S. Durot, C. Policar, F. Cisnetti, F. Lambert, J.-P. Renault, G. Pelosi, G. Blain, H. Korri-Youssoufi, J.-P. Mahy, *Eur. J. Inorg. Chem.* **2005**, 3513.

[69] L. Guijarro, M. Inclán, J. Pitarch-Jarque, A. Doménech-Carbó, J. U. Chicote, S. Trefler, E. García-España, A. García-España, B. Verdejo, *Inorg. Chem.* **2017**, *56*, 13748.

[70] D. Li, S. Li, D. Yang, J. Yu, J. Huang, Y. Li, W. Tang, *Inorg. Chem.* **2003**, *42*, 6071.

[71] R. Belda, S. Blasco, H. R. J. Begoña Verdejo, A. Doménech-Carbó, C. Soriano, J. Latorre, C. Terencio, E. García-España, *Dalton Trans.* **2013**, *42*, 11194.

[72] Q. Yuan, K. Cai, Z.-P. Qi, Z.-S. Bai, Z. Su, W.-Y. Sun, *J. Inorg. Biochem.* **2009**, *103*, 1156.

[73] S. Caglar, E. Adıgüel, B. Caglar, T. Saykal, E. Sahin, O. Büyügüngör, *Inorg. Chim. Acta* **2013**, *397*, 101.

[74] B. Dede, F. Karipcin, M. Cengiz, *J. Hazard. Chem.* **2009**, *163*, 1148.

SUPPORTING INFORMATION

Additional Supporting Information may be found online in the supporting information tab for this article.

How to cite this article: Tang Q, Wu J-Q, Li H-Y, Feng Y-F, Zhang Z, Liang Y-N. Dinuclear Cu(II) complexes based on *p*-xylylene-bridged bis(1,4,7-triazacyclononane) ligands: Synthesis, characterization, DNA cleavage abilities and evaluation of superoxide dismutase- and catalase-like activities. *Appl Organometal Chem*. 2018;e4297. https://doi.org/10.1002/aoc.4297